Ex vivo correction of severe coagulation Factor VII deficiency in patient-derived 3D liver organoids

Giacomo Roman,[1-3] Knut H. Lauritzen,[1-3] Sean P. Harrison,[4] Anindita Bhattacharya,[1-3] Marianne Seierstad Andresen,[2,3] Marie-Christine Mowinckel,[2,3] Barbora Smolkova,[4] Carola E. Henriksson,[1,5] Heidi Glosli,[4,6] Nina Iversen,[7] Bernd Thiede,[8] Gareth J. Sullivan,[4,9] Runar Almaas,[1,4] Per Morten Sandset,[1-3] Benedicte Stavik[2,3] and Maria E. Chollet[1-3]

[1]Institute of Clinical Medicine, University of Oslo, Oslo, Norway; [2]Department of Hematology, Oslo University Hospital, Oslo, Norway; [3]Research Institute of Internal Medicine, Oslo University Hospital, Oslo, Norway; [4]Department of Pediatric Research, Oslo University Hospital, Oslo, Norway; [5]Department of Medical Biochemistry, Oslo University Hospital, Oslo, Norway; [6]Center for Rare Disorders, Oslo University Hospital, Oslo, Norway; [7]Department of Medical Genetics, Oslo University Hospital, Oslo, Norway; [8]Department of Biosciences, University of Oslo, Oslo, Norway and [9]School of Medicine, University of St Andrews, St Andrews, UK

Correspondence: M.E. Chollet
m.e.c.dugarte@ous-research.no

Received: April 23, 2025.
Accepted: September 29, 2025.
Early view: October 9, 2025.

https://doi.org/10.3324/haematol.2025.288046

Abstract

Coagulation factor (F) VII deficiency is the most frequent among the rare, inherited bleeding disorders and is predominantly caused by missense mutations in the F7 gene. The disease phenotype ranges from asymptomatic cases to extremely severe hemorrhagic forms, requiring prophylactic injections with plasma-derived or recombinant FVII concentrates. In response, we have developed an autologous cell-based approach that corrects the disease-causing mutation in patient-derived induced pluripotent stem cells (iPSC) and generates therapeutic, three-dimensional hepatic organoids (HO). We report the CRISPR-mediated correction of homozygous c.718G>C (p.G240R), a missense mutation associated with a severe, life-threatening bleeding phenotype. The HO contain all liver cell types and exhibit key liver functions, including coagulation factor production. After correction, our data indicate that the patient-derived HO secrete consistent amounts of functional FVII protein, resulting in improved thrombin generation times. These results represent a significant milestone toward the establishment of an autologous cell-based therapy for patients with FVII- and other coagulation factor deficiencies.

Introduction

Coagulation factor (F) VII deficiency is an autosomal recessive disease resulting from a wide spectrum of mutations in the *F7* gene, located at 13q34.[1] It is the most frequent among the rare, inherited bleeding disorders, with an estimated prevalence of about 1:300'000 to 1:500'000, although an increased prevalence is reported in countries like Norway.[2] The clinical phenotype ranges from asymptomatic to severe-to-lethal hemorrhagic forms, which are often associated with early age of presentation.[3] Although the correlation between the clinical phenotype and the residual FVII coagulation activity (FVII:C) is poor, a relatively small increase in activity can alleviate symptoms.[1,4,5] The current treatment for FVII deficiency relies on protein replacement with frequent and highly expensive bolus injections of FVII concentrates, either recombinant or plasma-derived. Because FVII has a short half-life (less than 3 hours), patients with severe clinical phenotypes require very frequent, prophylactic injections and recurrent blood sampling for monitoring of treatment. In addition, the patients are also at risk of developing rare adverse events, such as inhibitors, i.e., antibodies neutralizing the exogenous FVII.[2,5]

The main variants responsible for inherited FVII deficiency are missense mutations, which account for about 78% of the total alterations in the *F7* gene.[6] We have previously reported a homozygous missense mutation in exon 8, the guanine (G) to cytosine (C) substitution at position 718 (c.718G>C, NM_000131.4; hg38 chr13: g.113117509G>C), in two Norwegian patients with residual FVII:C <1.0 IU/dL and spontaneous, intracranial hemorrhages.[2] This single-nucleotide change leads to the amino acid substitution of arginine for glycine at position 240 (p.G240R), resulting in impaired secretion and activity of FVII *in vitro*,[2] explaining the severe phenotype observed in patients.

By modulating the signaling pathways that regulate human hepatogenesis, induced pluripotent stem cells (iPSC) can

be successfully differentiated into functional hepatocytes.[7,8] We have recently reported how iPSC can be differentiated into advanced three-dimensional hepatic organoids (HO), which closely recapitulate the structural and functional complexity of the human liver.[9] The HO are composed of both parenchymal (hepatocytes and cholangiocytes) and non-parenchymal cell types (hepatic stellate cells, Kupffer cells and liver sinusoidal endothelial cells). They show advanced competency in synthesizing and secreting coagulation factors, such as FVII, and coagulation inhibitors, such as antithrombin, and we have demonstrated that HO can secrete human liver proteins into the circulation following transplantation/engraftment in mice.[9]

In this study, we corrected the FVII mutation p.G240R in patient-derived iPSC using clustered regularly interspaced short palindromic repeats (CRISPR) and CRISPR-associated protein 9 (Cas9) technology and then differentiated both patient and gene-corrected iPSC into functional HO. We demonstrate that both production and secretion of functional FVII protein were restored in the corrected patient-derived HO. This study represents a significant advancement in the development of an autologous cell-based therapy for severe FVII deficiency, which is potentially applicable to other inherited deficiencies of coagulation factors.

Methods

The study was approved by the Norwegian regional committees for medical and health research ethics (REK 2018/777) and the data protection officer at Oslo University Hospital (PVO #18/20935), and was conducted in accordance with the Declaration of Helsinki.

The extended methods are present in the *Online Supplementary Appendix*.

Generation and culturing of patient-derived induced pluripotent stem cells

Peripheral blood mononuclear cells (PBMC) were reprogrammed to iPSC using the CytoTune-iPS 2.0 Sendai Reprogramming Kit (Thermo Fisher Scientific; MA, USA).

Tri-lineage assessment of pluripotency

The iPSC were directed to the definitive endoderm using the protocol developed by Mathapati *et al.*[10] and Harrison *et al.*[9] to mesoderm using the protocol from Lian *et al.*[11] and to ectoderm employing the method described by Chambers *et al.*[12] and Maroof *et al.*.[13]

CRISPR gene editing

The gene editing experiments were performed by nucleofection (Neon transfection system, Thermo Fisher Scientific) of ribonucleoprotein (RNP) complexes, assembled following IDT's recommendations (IDT; Newark, NJ, USA).

Droplet digital polymerase chain reaction

The droplet digital polymerase chain reaction (ddPCR) was performed using customized NHEJ and HDR Genome Edit Detection Assays on a QX200 System and analyzed using QX Manager Software, v2.1 (Bio-Rad; CA, USA).

Immunofluorescence and microscopy

Immunofluorescence analyses were performed following Harrison *et al.*, 2023[9] for the HO and the Cell Signaling protocol (MA, USA) for the iPSC, and using ECHO Revolve RVL-100-M, Zeiss LSM 880 Airyscan FAST and Andor Dragonfly Spinning Disk confocal microscopes.

Sanger sequencing and whole exome sequencing

Sanger sequencing, whole exome sequencing (WES) analyses at 30x (Clinical Research Exome) and 100x coverage and downstream bioinformatic analysis were performed by Eurofins Genomics (Ebersberg, Germany).

Hepatic organoid differentiation

HO were generated using the protocol developed by Harrison *et al.*.[9] On day 19, the HO were incubated with serum-free L-15 medium, supplemented with 5 µg/mL Vitamin K1. Both HO and the cell supernatant were collected on day 21 for downstream analyses, after 2 days in serum-free conditions.

Protein determination and activity assay

FVII protein levels and activity were analyzed by U-PLEX Human Factor VII (Meso Scale Diagnostic; MD, USA) and BIOPHEN FVII assay (Hyphen BioMed; Neuville-sur-Oise, France), respectively. Factor X, albumin and α-1 antitrypsin (A1AT) antigens were measured by enzyme-linked immunosorbent assay (ELISA). Thrombin generation was assessed by calibrated automated thrombogram (CAT) (Diagnostica Stago; Asnières-sur-Seine, France), by mixing HO supernatant with FVII-deficient plasma. Total protein was quantified with Pierce BCA Protein Assay Kits (VWR; Radnor, PA, USA).

Liquid chromatography-mass spectrometry analysis

Liquid chromatography-mass spectrometry (LC-MS) was performed on SDS-PAGE bands using a timsTOF Pro spectrometer (Bruker Daltonik; Bremen, Germany). Data analysis was performed using Scaffold v5.1.2 (Proteome Software Inc.; OR, USA).

Statistical analyses

The statistical analyses and graphs were performed with GraphPad Prism 10.2.0. The data were generated from three independent experiments consisting of two biological replicates for the HO and one for the PH and are expressed as mean and standard deviation. The normal distribution was assessed by Shapiro-Wilk test. For the comparison among two groups the statistical significance was determined by unpaired Student's *t* test. A probability value of $P<0.05$ was considered statistically significant.

Results

Generation and characterization of patient-derived induced pluripotent stem cells

The primary PBMC isolated from the peripheral blood of the FVII-deficient patient were reprogrammed to iPSC using Sendai virus and, on appearance of iPSC colonies, clones were picked based on correct morphology. After passaging of clones for 10 to 12 passages we demonstrated the complete clearance of any residual Sendai reprogramming factor, compared to PBMC 3 days after transduction (Figure 1A). After 20 passages, genetic stability was investigated by karyotyping, revealing no evidence of aneuploidy or rearrangements (Figure 1B). To corroborate this further and profile the patient-derived iPSC genetic background, whole exome sequencing was performed. When mapped against the GRCh38 reference assembly and filtered according to allele frequency (AF) ≥0.01 and read depth (DP) ≥20, no

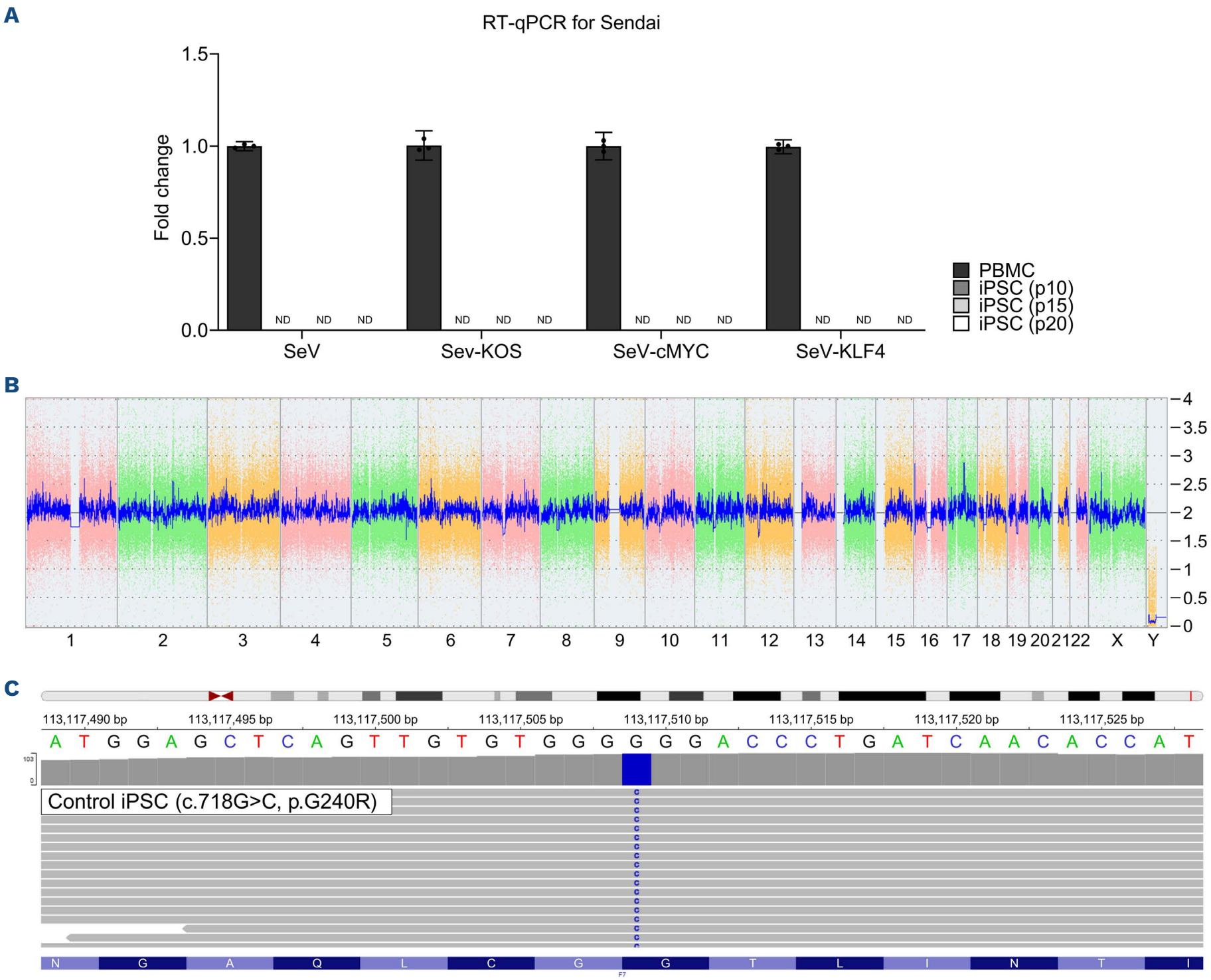

Figure 1. Genetic characterization of patient-derived induced pluripotent stem cells (c.718G>C, p.G240R). (A) Quantitative real-time polymerase chain reaction (RT-qPCR) to assess Sendai clearance, using 18S endogenous control. Peripheral blood mononuclear cells (PBMC) after 3 days from transduction were used as a positive control. Results are expressed as mean ± standard deviation (N=3). "Not detected" (ND) indicates undetermined Ct values. (B) KaryoStat+ Assay Report. The whole genome view displays all somatic and sex chromosomes in one frame with high-level copy number. The smooth signal plot (right, y-axis) is the smoothing of the log2 ratios which depict the signal intensities of probes on the microarray. A value of 2 represents a normal copy number state (CN=2). A value of 3 represents chromosomal gain (CN=3). A value of 1 represents a chromosomal loss (CN=1). The pink, green and yellow colors indicate the raw signal for each individual chromosome probe, while the blue signal represents the normalized probe signal. (C) Integrative Genomics Viewer (IGV; igv.org) view from the Illumina WES INVIEW Human Exome 100x analysis. Sequencing reads are presented in grey, the GRCh38/hg38 reference sequence is located at the top, under the chromosomal coordinates. c.718G>C mismatch is presented in blue. iPSC: induced pluripotent stem cells.

relevant short variants, such as single nucleotide variants (SNV) or small insertions/deletions (InDels), were detected in the *F7* gene, but only the c.718G>C missense SNV corresponding to the severe p.G240R mutation (Figure 1C). Next, pluripotency was examined in the confirmed Sendai-free iPSC, first by assessing the pluripotency markers OCT4, NANOG and SOX2 by immunofluorescence, and expression of all markers was detected (Figure 2A, B). We then assessed tri-lineage potential by differentiating the iPSC into the three germ layers. We assessed endoderm potential by differentiating to definitive endoderm, producing iPSC that were FOXA2$^+$/SOX17$^+$ double-positive, during both 3 μM and 4 μM CHIR99021 conditions (Figure 2C). Further gene expression analyses demonstrated that all the conditions exhibited the upregulation of both *FOXA2* and *SOX17* endoderm-specific markers (Figure 2D). When differentiated to the ectoderm lineage, the resulting neuroepithelium was NESTIN$^+$/SOX2$^+$/PAX6$^+$ positive (Figure 2E), a combination of markers specific for neural progenitor cells.[14] Using real time (RT)-qPCR we showed a 47-fold upregulation of *PAX6* expression (Figure 2F). For mesoderm, we differentiated iPSC to cardiomyocytes, and after 2 weeks we observed spontaneously contracting cardiomyocytes, from 24x10^3 and 36x10^3 iPSC/cm^2 under both 8 μM and 10 μM CHIR99021 (*Online Supplementary Video S1*). We further validated by assessing the cardiac-specific marker Cardiac Troponin I (cTnI) which we observed (Figure 2G), as well as significant upregulation of Troponin T2 (*TNNT2*), used as a cardiac-specific mRNA marker for all the different differentiation conditions (Figure 2H). We observed the *TNNT2* upregulation up to 40-fold, in cardiomyocytes from 36x10^3 iPSC/cm^2 under 8 μM CHIR99021 (Figure 2H).

Gene correction of *F7* c.718G>C missense mutation and induced pluripotent stem cell cloning

To gene edit c.718G>C, six different gRNA were designed *in silico* (*Online Supplementary Figure S1A*). Following nucleofection, the intracellular presence of the CRISPR RNP was verified by fluorescent microscopy (*Online Supplementary Figure S1B*). The on-target cutting activity of each gRNA was evaluated post nucleofection using the ddPCR. The analysis of non-homologous end joining (NHEJ) event by ddPCR indicated a fractional abundance, i.e., the ratio edited alleles (FAM$^+$/HEX$^-$ droplets)/total alleles (FAM$^+$, FAM$^+$/HEX$^+$), of 41% and 48% for gRNA #2 and gRNA #5, respectively, meaning that ~50% of the population of alleles carried a NHEJ event (*Online Supplementary Figure 1C, D*). The corresponding values for the negative control, consisting of CRISPR components nucleofected without gRNA, was 0% (*Online Supplementary Figure S1C, D*). As a result, gRNA #5 was chosen as an ideal candidate to perform gene correction of *F7* c.718G>C in patient-derived iPSC (*Online Supplementary Figure S2A*). For the correction we leveraged homology-directed repair (HDR), we explored how efficiency was influenced under different concentrations of the HDR enhancer V2. Using ddPCR analyses we observed HDR rates ranging from 19.4% (no enhancer) up to 50.7% (1 μM V2 HDR enhancer) (*Online Supplementary Figure S2B, C*). To maximize the HDR rate while minimizing the concentration of V2 HDR enhancer, we selected CRISPR HDR pools with 0.25 μM HDR enhancer. From this, single cell-derived iPSC clones were then successfully generated. A detailed monoclonality report was generated for each single cell (*Online Supplementary Figure S3*) by combining the sorting data with the clonal iPSC follow-up by plate imaging. The impedance signals were analyzed to meet highly stringent quality criteria, such as optimal particle size (≥400 and ≤3,000 ohm) and low background signal noise, during both detection and dispensing. No sign of differentiation and/or morphological abnormalities in the single cell-derived iPSC colony were identified. iPSC that passed these criteria were then screened for HDR occurrence at the target locus by Sanger sequencing, which also functioned as an initial screen for monoclonality (Figure 3A).

Off-target analysis and whole exome sequencing

We next assessed potential off-target sites predicted by Benchling (Benchling; San Francisco, CA, USA) and IDT using WES. We cross-checked with the variant calling report, generated by filtering the comparison between the original patient iPSC line carrying the c.718G>C mutation (control) against corrected iPSC clones. With AF ≥0.01 and DP ≥20, we observed no off-target effects, relevant and/or deleterious variants possibly associated with CRISPR editing (*Online Supplementary Table S2*). The WES confirmed the correction of c.718G>C was present at 100%, with 45x coverage (Figure 3B). This also further validated monoclonality of the corrected iPSC clone.

Differentiation to hepatic organoids and *in vitro* assessment of FVII production

Both patient and corrected iPSC were differentiated into HO (Figure 4A-C). To investigate FVII production in HO we generated iPSC-derived HO as described by Harrison *et al.*[9] We assessed efficiency and quality of the differentiation at day 6 by measuring the expression of the hepatic marker HNF4A. Both p.G240R control and corrected HO were positive for HNF4A (Figure 4B). Upon the QC stage the HO were cultured until day 19 when they reached a mature state and presented with liver-like cellular complexity. At day 21 we assessed the markers HNF4A and asialoglycoprotein receptor 1 (ASGR1), a marker for mature hepatocytes,[9,15] by immunofluorescence (Figure 4C). We next assessed the HO for key hepatic attributes at the transcriptional level. Using RT-qPCR we verified the presence of hepatic markers *HNF4A* and two cytochrome P450 (*CYP450*) enzymes, *CYP3A4* and *CYP3A7* (Figure 4D). When compared to p.G240R control HO and primary hepatocytes (PH), the corrected HO showed increased transcription of *HNF4A*, of about ~2-fold (P<0.001). Interestingly, *CYP3A4* expression in corrected HO was in-

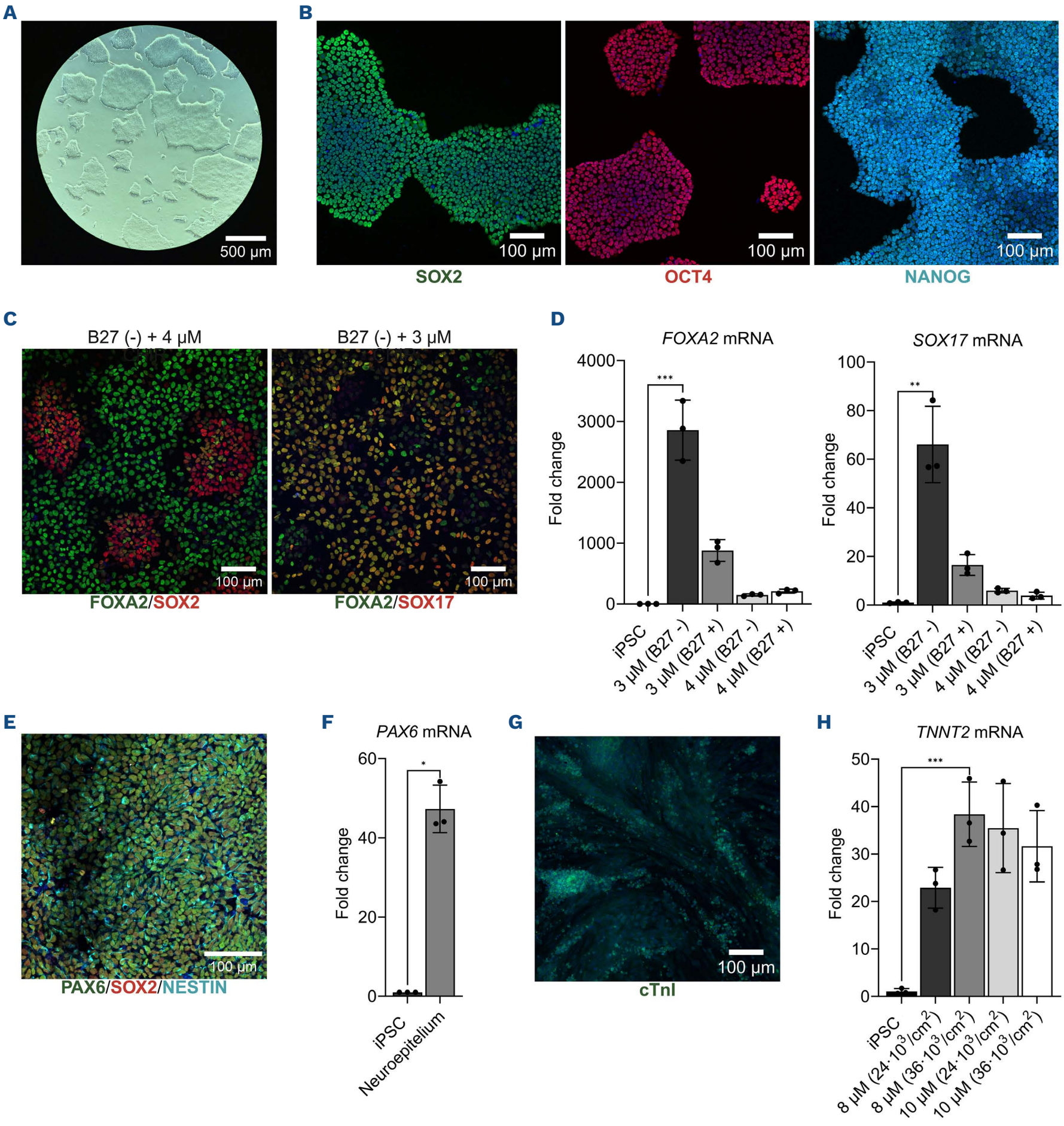

Figure 2. Functional characterization of induced pluripotent stem cell pluripotency by tri-lineage differentiation assay. (A) Bright-field image of the selected induced pluripotent stem cell (iPSC) clone (500 µm scale bar). (B) Immunofluorescence analysis on the selected iPSC clone for pluripotency markers (from left) SOX2 (green), OCT4 (red), and NANOG (cyan) (100 µm scale bar). Zeiss LSM 880 Airyscan FAST confocal microscope. (C, left) Immunofluorescence analysis on the iPSC-derived definitive endoderm for FOXA2 (green) and SOX2 (red), cultured with B27- + 4 µM CHIR. (C, right) FOXA2 (green) and SOX17 (red), for the iPSC-derived definitive endoderm cultured with B27- + 3 µM CHIR (100 µm scale bar). (D) Real-time polymerase chain reaction (RT-qPCR) analysis of definitive endoderm-associated markers *FOXA2* and *SOX17*, using 18S endogenous control. iPSC (p22) were used as a control. Results are expressed as mean ± standard deviation (SD) (N=3). Statistical significance was determined by unpaired *t* test, with ***P<0.001 and **P<0.01. (E) Immunofluorescence analysis on the iPSC-derived neuroepithelium, for PAX6 (green), SOX2 (red) and NESTIN (cyan) (100 µm scale bar). (F) Quantitative RT-qPCR analysis of *PAX6* expression, in the iPSC-derived neuroepithelium. Results are expressed as mean ± SD (N=3), *P<0.05 with unpaired *t* test. (G) Immunofluorescence analysis on the iPSC-derived cardiomyocytes, for cTnI (green) (100 µm scale bar). (H) Quantitative RT-qPCR analysis of *TNNT2* expression. Results are expressed as mean ± SD (N=3), ***P<0.001 with unpaired *t* test.

creased by ~10.1-fold (P<0.01) when compared to control p.G240R HO but reduced to ~0.12-fold when compared to PH (Figure 4D). In contrast, *CYP3A7* expression in corrected HO was downregulated ~6.5-fold, when compared to control p.G240R HO (P<0.001). We then assessed the production and secretion of two liver-specific proteins, albumin (ALB) and α-1-antitrypsin (A1AT) by ELISA (Figure 4E). While we detected similar amounts of secreted ALB, A1AT secretion was decreased by ~1.79-fold in the corrected HO, when compared to the control p.G240R HO (P<0.01) (Figure 4E). We also assessed *F10* at the mRNA level and FX antigen levels (FX:Ag) (Figure 5A), where we observed no significant differences in levels after correction of the *F7* mutation.

Finally, we investigated FVII production in HO. First, we found that *F7* transcription in the corrected HO increased by ~1.39-fold fold, when compared to control p.G240R (P<0.01) (Figure 5B). Next, we examined intracellular FVII synthesis by quantitative U-PLEX FVII assay and immunostaining. Corrected HO exhibited a 9-fold increase (P<0.0001) in the intracellular FVII levels, reaching 1.32±0.32 pg/µg total protein when compared to control p.G240R HO (0.14±0.009 pg/µg total protein) (Figure 5B). Immunostaining confirmed the presence of intracellular FVII in both control p.G240R and corrected HO (Figure 5C). Notably, while we could detect both *F7* transcript and intracellular FVII protein in the control p.G240R HO, no FVII antigen was found in the supernatant measured by U-PLEX FVII assay. On the other hand, the corrected HO secreted 3.97±1.1 pg/µg total cellular protein, thus confirming that the gene correction successfully restored both physiological FVII synthesis and

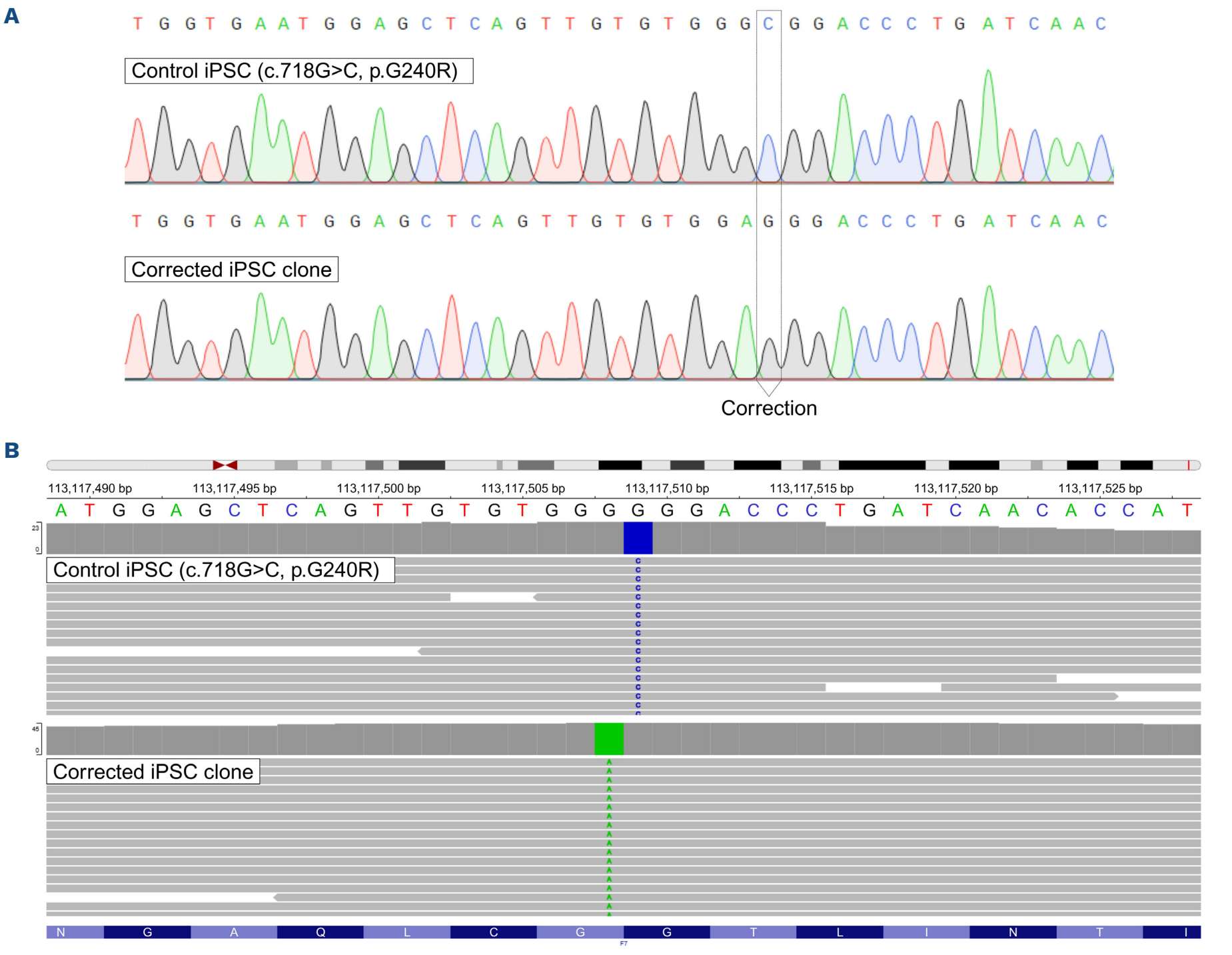

Figure 3. Genetic characterization of a gene-corrected, single cell-derived induced pluripotent stem cell clone. (A) Sanger sequencing view of gRNA #5/ssODN donor-targeted locus, at exon 8 of F7. c.718G>C, p.G240R control (top) and a homozygous, corrected induced pluripotent stem cell (iPSC) clone (bottom). Generated with SnapGene® Viewer 7.2.1. (B) Integrative Genomics Viewer (IGV; igv.org) view from the Illumina Clinical Research Exome - CRE V4 analysis. Sequencing reads are presented in grey, the GRCh38/hg38 reference sequence is located at the top, under the chromosomal coordinates. c.718G>C, p.G240R control (top) and a homozygous, corrected iPSC clone (bottom).

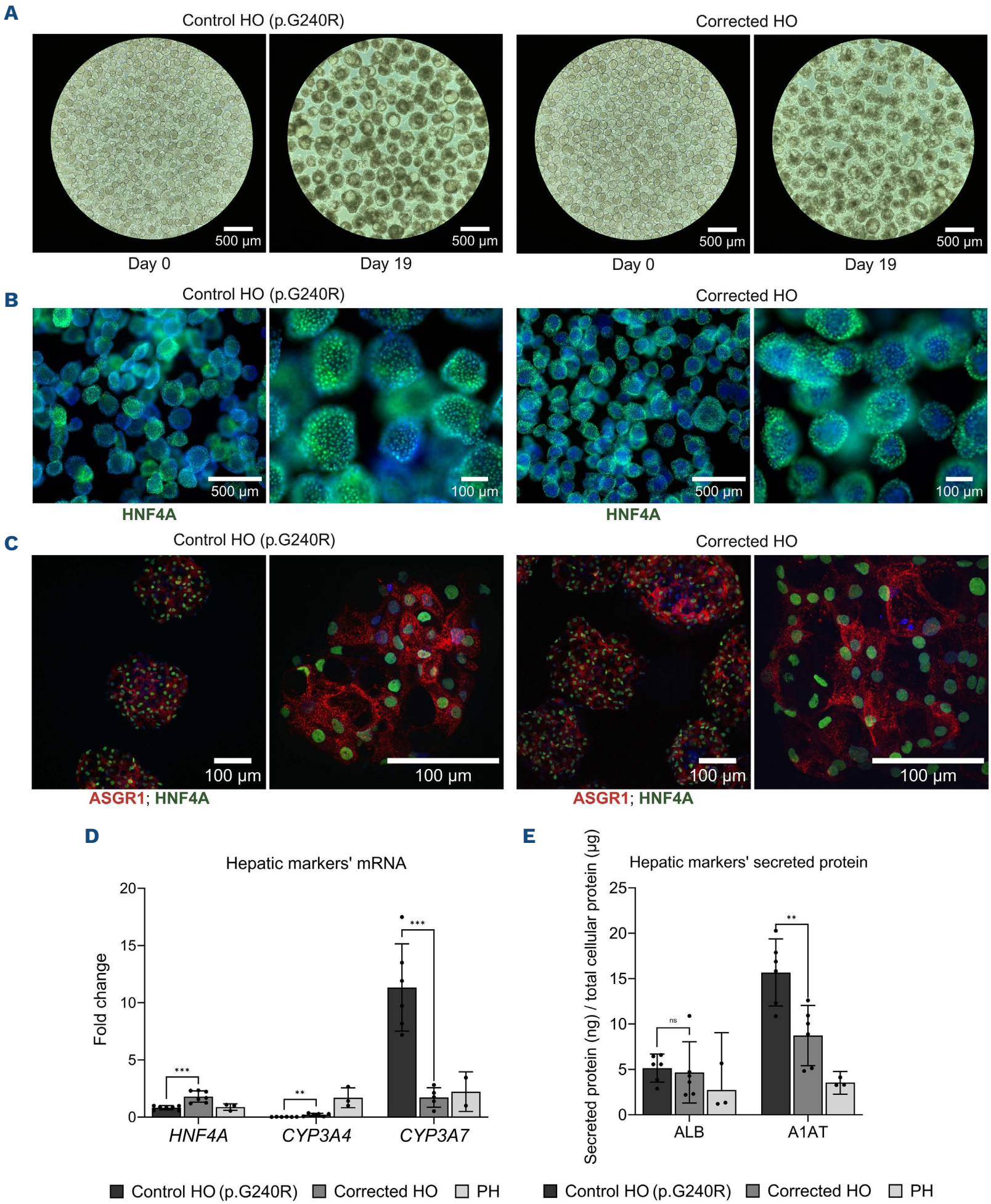

Figure 4. Generation and characterization of p.G240R control and corrected hepatic organoids. (A) Brightfield images of p.G240R control (left) and corrected hepatic organoids (HO) (right), at day 0 and day 19 of the differentiation (500 µm scale bar). ECHO Revolve RVL-100-M. (B) Immunofluorescence analysis for HNF4A marker on p.G240R control (left) and corrected HO (right), at day 6 (500 µm and 100 µm scale bars). ECHO Revolve RVL-100-M. (C) Immunofluorescence analysis for ASGR1 and HNF4A markers on p.G240R control (left) and corrected HO (right), at day 19 (100 µm scale bar). Andor Dragonfly Spinning Disk confocal microscope. (D) Quantitative real-time polymerase chain reaction (RT-qPCR) analysis of *HNF4A*, and 2 enzymes of the *CYP450* enzyme family, *CYP3A4* and *CYP3A7* (from left to right), using 18S endogenous control. Results are normalized to primary hepatocytes (PH) and expressed as mean ± standard deviation (SD). Statistical significance was determined by unpaired *t* test, with **P*<0.05 and *****P*<0.0001. (E) ALB and A1AT quantification by enzyme-linked immunosorbent assay. Results were normalized to the total cellular protein and adjusted to the culture volume, and expressed as mean ± SD. Statistical significance was determined by unpaired *t* test, with ***P*<0.01.

secretion (Figure 5B). We next conducted liquid chromatography-mass spectrometry (LC-MS) analyses on the culture supernatants and lysates derived from two independent experiments of both control p.G240R and corrected HO (Figure 6). After SDS-PAGE separation, we excised gel fragments between 40-60 kDa, corresponding to the expected

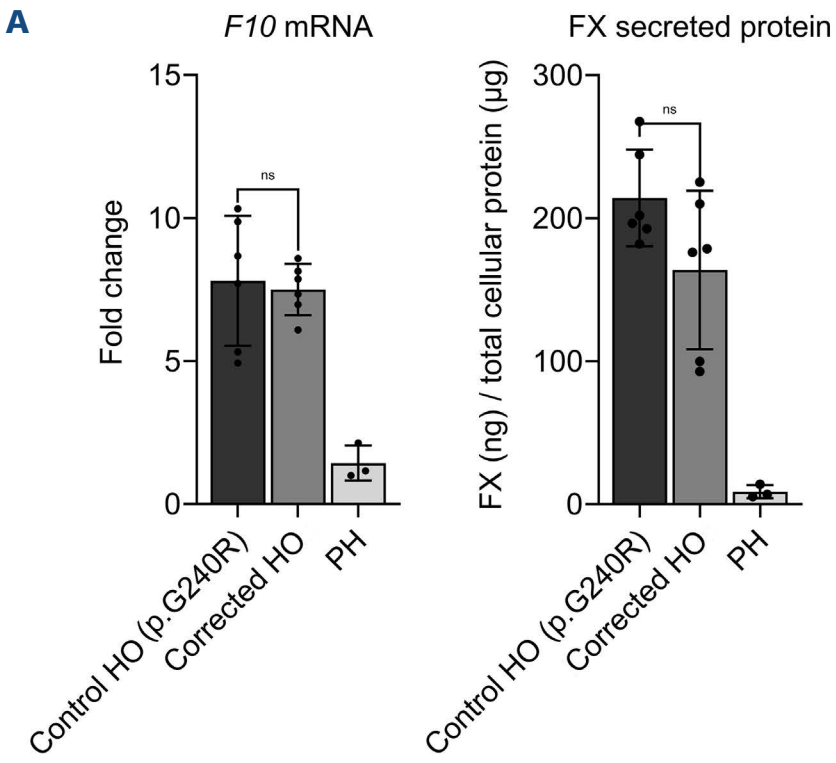

Figure 5. FX and FVII analysis. (A, left) Real-time polymerase chain reaction (RT-qPCR) analysis of *F10* expression, using 18S endogenous control. Results are normalized to primary hepatocytes (PH) and expressed as mean ± standard deviation (SD). Statistical significance was determined by unpaired *t* test. (A, right) FX antigen quantification by enzyme-linked immunosorbent assay (ELISA). Results were normalized to the total cellular protein and adjusted to the culture volume, and expressed as mean ± SD. Statistical significance was determined by unpaired *t* test. (B, left) Quantitative RT-qPCR analysis of *F7* expression, using 18S endogenous control. Results are normalized to PH and expressed as mean ± SD. Statistical significance was determined by unpaired *t* test, with ***P*<0.01. (B, middle) Intracellular FVII antigen quantification by U-PLEX assay. Results were normalized to the total cellular protein and expressed as mean ± SD. Statistical significance was determined by unpaired *t* test, *****P*<0.0001. (B, right) Secreted FVII antigen quantification by U-PLEX assay. Results were normalized to the total cellular protein and adjusted to the culture volume, and expressed as mean ± SD. "Not detected" (ND) indicates values below the assay detection limit. (C) Immunofluorescence analysis for FVII and HNF4A markers on p.G240R control (left) and corrected hepatic organoids (HO) (right), at day 19 (100 µm scale bar, Andor Dragonfly Spinning Disk confocal microscope).

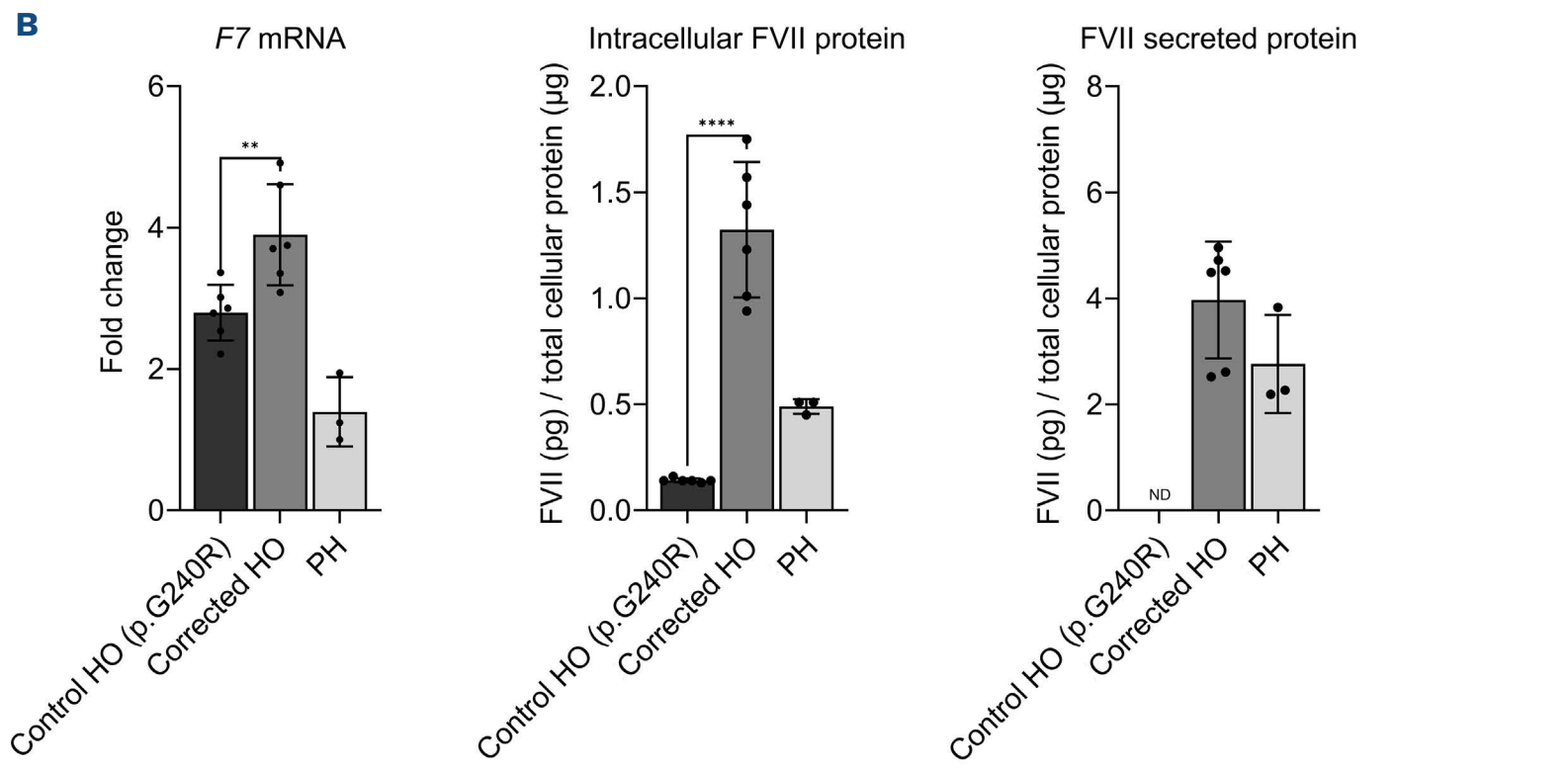

A Corrected HO (Supernatant)

6 exclusive unique peptides, 7 exclusive unique spectra, 9 total spectra, 83/466 amino acids (18% coverage)

5 exclusive unique peptides, 6 exclusive unique spectra, 6 total spectra, 72/466 amino acids (15% coverage)

B Control HO (p.G240R) (Lysate)

2 exclusive unique peptides, 2 exclusive unique spectra, 2 total spectra, 22/466 amino acids (5% coverage)

C Corrected HO (Lysate)

4 exclusive unique peptides, 4 exclusive unique spectra, 4 total spectra, 59/466 amino acids (13% coverage)

5 exclusive unique peptides, 5 exclusive unique spectra, 6 total spectra, 72/466 amino acids (15% coverage)

D PH (Supernatant)

2 exclusive unique peptides, 2 exclusive unique spectra, 2 total spectra, 36/466 amino acids (8% coverage)

Figure 6. Liquid chromatography-mass spectrometry analysis. (A) Sequence coverage from the liquid chromatography-mass spectrometry analysis of the corrected induced pluripotent stem cell (iPSC) supernatants (40-60 kDa samples, positive for FVII), (B) the control hepatic organoids (HO) (p.G240R) lysate (40-60 kDa), (C) the corrected HO lysates (40-60 kDa) and (D) the primary hepatocytes (PH) supernatant (40-60 kDa). Identified matching peptide sequences are highlighted in yellow and bold.

molecular weight of FVII (~52 kDa) (*Online Supplementary Figure S9*). FVII peptides were identified in the corrected HO supernatants, with sequence coverage of 18% and 15%, respectively (Figure 6A). In contrast, no FVII peptides were detected in the control p.G240R HO supernatants. As a positive reference, PH supernatant showed detectable FVII peptides with 8% sequence coverage (Figure 6D). In the lysate fraction, FVII peptides were found in both corrected HO samples (13% and 15% coverage) (Figure 6C), and in one of the two p.G240R control HO lysates (5% coverage) (Figure 6B).

To address the functional activity of the FVII produced, we investigated the ability of secreted FVII to activate FX, in presence of thromboplastin. We detected an absolute FVII chromogenic activity of 0.053±0.012% of plasma calibrator in the corrected HO (Figure 7A). In this context, corrected HO secreted 0.41±0.15 ng/mL of FVII:Ag, while control p.G240R HO remained negative (not detected [ND]) and PH (positive control) secreted 1.32±0.12 ng/mL (Figure 7A). As positive references, PH and pooled normal plasma (PNP) reached 0.93±0.19 and 121.2% of plasma calibrator, respectively. Additionally, we included HO derived from a healthy, unedited and wild-type (WT) iPSC line (AG27),[9] which showed an absolute chromogenic activity of 0.086% of plasma calibrator and served as a more suitable iPSC-derived HO control system (Figure 7A). The corresponding specific FVII activity, i.e., the relative functional output of the secreted protein, of the corrected HO was 1.38±0.32 mIU/ng FVII. In contrast, control p.G240R HO and L-15 medium control remained negative (ND) (Figure 7B). The AG27 WT HO showed a specific activity of 0.825±0.01 mIU/ng, while PH and PNP reached 7.06±0.89 mIU/ng and 7.66 mIU/ng, respectively (Figure 7B). To further expand on the functional characterization of the rescued FVII, we also performed a thrombin generation assay to assess the overall hemostatic potential of the secreted FVII in a dynamic, plasma-based system (Figure 7C, D). Results showed that the lag time was reduced from 16.22±0.8 to 12.05±0.49 (P<0.0001) in the corrected HO compared to the p.G240R control, when triggered with the standard 5 pM tissue factor (TF) (Figure 7C). To further challenge the sensitivity and dynamics of the assay, we repeated the test using 1 pM of TF trigger. The results confirmed our previous findings, with a prolonged lag time of 20.67 ±2 in the p.G240R control *versus* 16.07±1.3 in the corrected HO (P<0.001) (Figure 7D).

Discussion

Here we report the successful *ex vivo* correction of a severe FVII deficiency, providing *in vitro* proof-of-concept evidence for the potential development of a cell-based therapy approach using autologous HO for treatment of these patients. As demonstrated by pioneering studies on hemophilia A and B,[16-20] different CRISPR-Cas9 editing strategies have been used to correct mutations in *F8* and *F9* genes, and produce gene-corrected patient-derived iPSC for further therapeutic purposes, but to date this approach has not been used to restore FVII function. Currently, over 271 different pathogenic variants within the *F7* gene have been reported by the European Association for Hemophilia and Allied Disorders (EAHAD) database,[21] with the majority being missense mutations. For this reason, we present the rescue of the debilitating missense c.718G>C variant, encoding a p.G240R substitution in the catalytic domain of FVII,[2,22-24] where more than half of the mutations are found,[2,21] which causes a very severe clinical phenotype. In addition, another variant, the c.718G>A missense mutation, encodes the same amino acid substitution (p.G240R) and has been described in three different studies, two of which report a homozygous c.718G>A ,that causes fatal, intracranial hemorrhaging.[22-24] The patients with homozygous c.718G>A had undetectable FVII:Ag and FVII:C <1.0 IU/dL. Thus, the chosen mutation has shown consistency in phenotype severity across affected individuals and emerges as an ideal candidate for such therapy.

Efficacy and safety are central considerations in the advancement of CRISPR- and cell-based therapies.[25] In this study, we show that it is possible to streamline the pipeline for generating autologous cell products for FVII deficiency without mitigating efficacy or safety. Firstly, we demonstrate robust reprogramming of somatic cells (PBMC) into iPSC, without causing any observable genome instability or the introduction of mutations in protein coding genes. Secondly, we demonstrate efficient and safe gene correction, with no CRISPR-related off-target effects or relevant, deleterious modifications identified. The transient delivery of the Cas9 nuclease/gRNA as an RNP complex, ensures that the Cas9 is active immediately upon entering the cell and rapidly cleared from the cell, maximizing on-target activity and minimizing off-target effects.[26,27] In contrast, plasmid-based methods require extended time for the CRISPR components to be synthesized and be active on-target. For this reason, they typically associate with Cas9 persistence over time (>72 hours), which significantly increases the risks of off-target effects and leads to unpredictable variability, due to Cas9 and gRNA expression levels.[26,28] Although newer CRISPR tools such as prime editing and base editing are emerging and have been utilized for gene editing both *in vitro* and *in vivo* (mouse),[29-31] the nuclease-based CRISPR-Cas9 technology has recently received Food and Drug Administration approval for the treatment of sickle cell disease and β-thalassemia, demonstrating its safety and potential for clinical use.[32] Thirdly, as the exposure to CRISPR-Cas9 may result in mixed populations of cells harboring different editing outcomes, the establishment of stable, monoclonal iPSC lines with a defined genotype is particularly important from a safety point of view. Using an impedance-based system that allows for the single-cell detection and gentle dispensing (≤2 psi) of the iPSC, we

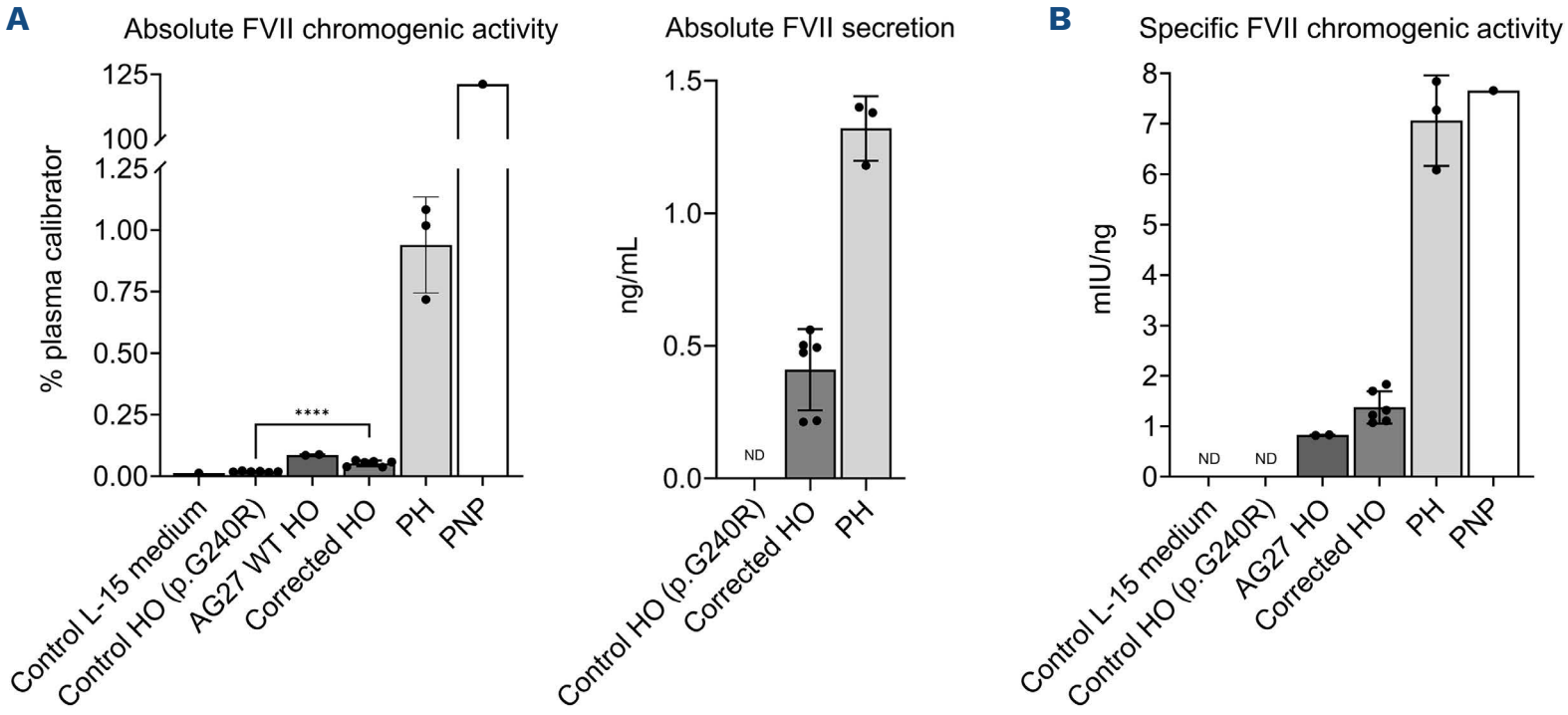

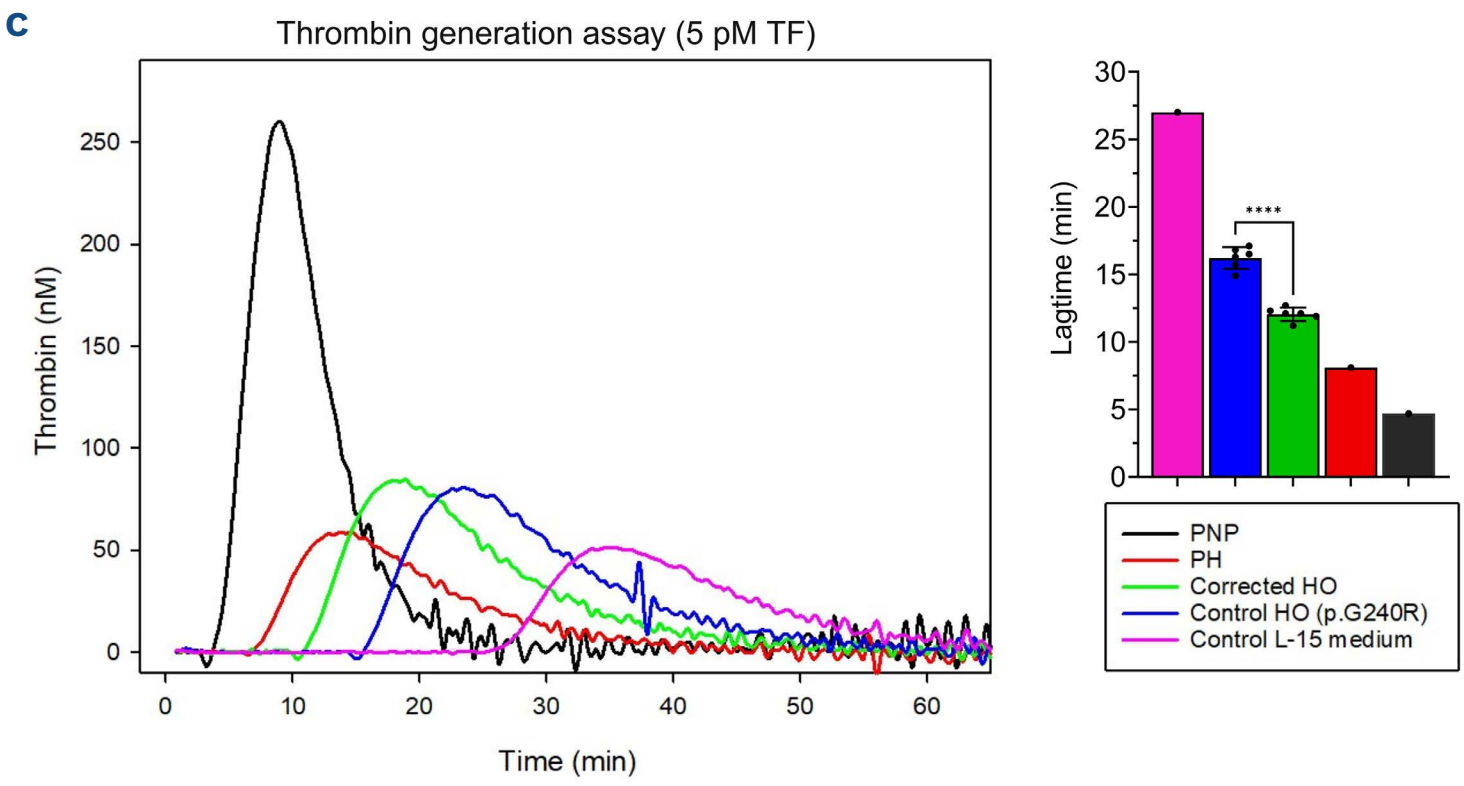

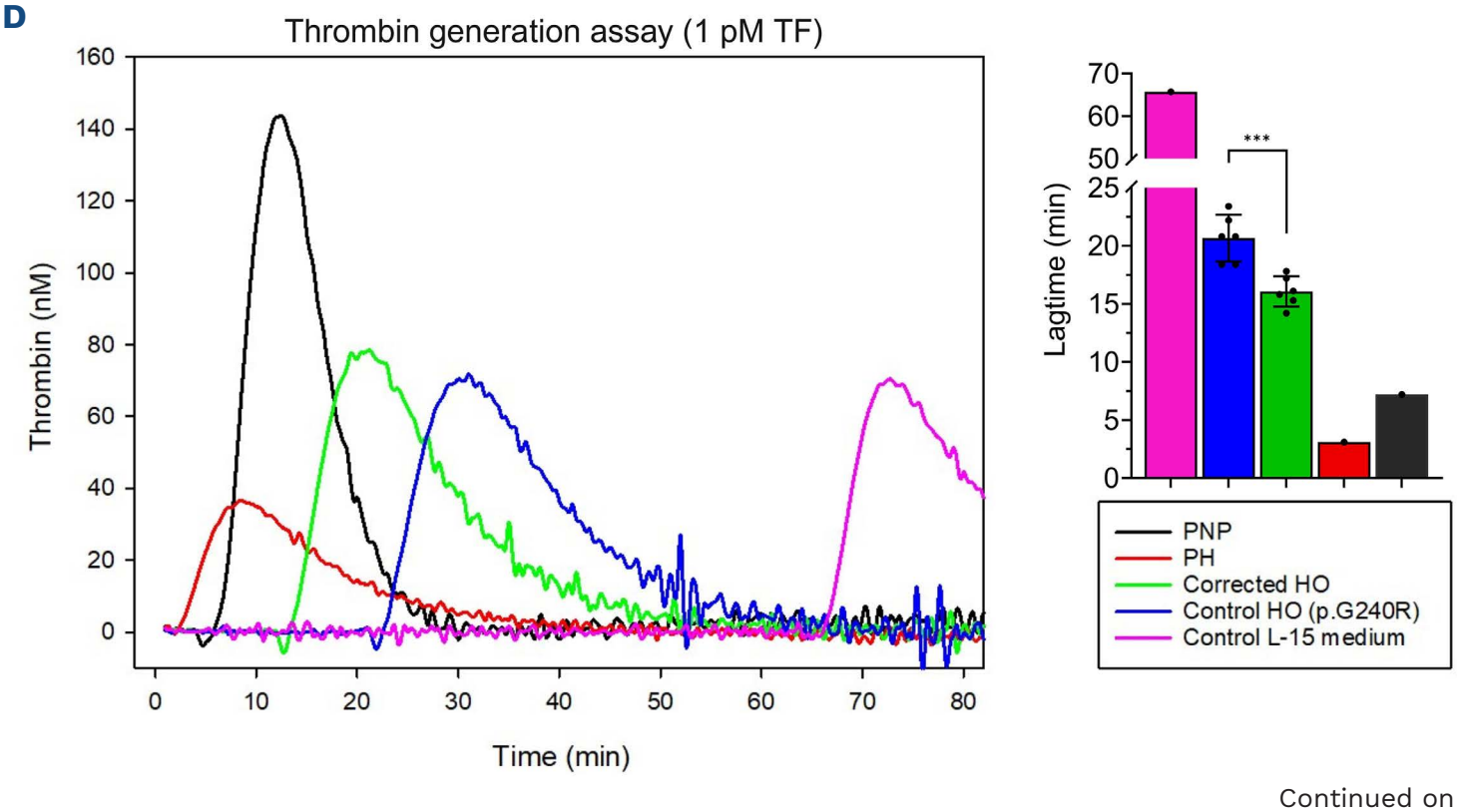

Continued on following page.

Figure 7. FVII activity and total coagulation analyses. (A, left) BIOPHEN FVII analysis to determine absolute FVII chromogenic activity in cell culture supernatant. Results were expressed as % of plasma assay calibrator and as mean ± standard deviation (SD). Statistical significance was determined by unpaired *t* test, ****P<0.0001. (A, right, up) Quantification of FVII absolute secretion by U-PLEX assay. Results were expressed in ng/mL, as mean ± SD. (B) Specific FVII chromogenic activity calculated by dividing the activity in mIU by the corresponding antigen level in ng. The conversion from % activity to IU (FVII:C) was based on Mathijssen *et al*..[44] "Not detected" (ND) indicates values below the assay detection limit. (C) Thrombin generation assay using 5 pM TF trigger. (D) Thrombin generation assay using 1 pM TF trigger. Results were expressed in minutes, as mean ± SD. Statistical significance (for samples with N=6) was determined by unpaired *t* test, with ***P<0.001 and ****P<0.0001. HO: hepatic organoids; PNP: pooled normal plasma; PH: primary hepatocytes.

demonstrate high-throughput and rapid single-cell cloning of edited cells without having to rely on manual colony picking, limiting dilution, or fluorescence-activated cell sorting that are less efficient, labor-intensive and more obtrusive.[33-35] The resulting monoclonality also provides a key advantage for genome assessment, as any variant or editing-associated effect would be uniformly represented across the entire cell population, enhancing detection sensitivity. For this reason, the WES coverage and filtering criteria employed in this study provided confident detection of coding variants, offering reliable detection of potential off-target effects within protein-coding genes. However, we recognize the importance of expanding this analysis to WGS to achieve a more comprehensive, base-pair resolution profile, including non-coding or regulatory regions not fully captured by WES. Such in-depth analysis would further strengthen the safety assessment of genome-edited cell lines, particularly in the context of future clinical translation.

We have reported that p.G240R control and CRISPR-corrected iPSC undergo HO differentiation with similar efficiency and yield, with both expressing key liver markers and secreting liver-specific proteins. Although ALB and FX secretion levels were comparable, we observed increased *HNF4A* and *CYP3A4* expression, as well as decreased *CYP3A7* transcription and A1AT secretion in the corrected HO. While these findings may suggest features of hepatic zonation or mature phenotype and FVII has been associated with coagulation-independent effects in the liver,[9,36,37] they remain to be further investigated. Most notably, the gene correction strategy successfully rescued the FVII deficient phenotype in patient-derived HO *ex vivo*. Consistent with the previous evidence,[2] we demonstrated by RT-qPCR, U-PLEX and LC-MS analyses that the c.718G>C (p.G240R) variant does not abolish transcription and translation of FVII, but associates with severely impaired protein secretion. In contrast, the correction enabled the secretion of biologically functional FVII. Although the corrected HO showed a substantial increase in FVII secretion compared to the p.G240R control, the corresponding increase in activity was comparatively modest, particularly when compared to the PH and PNP positive controls. The reason for this is not known, but it aligns with previous observations on the broader challenge of detecting the activity of vitamin K-dependent proteins *in vitro*, which might be affected by rapid protein degradation, dilution in the supernatant volume, as well as several other factors, such as culture medium and incubation time.[19,38,39] Whether the modest FVII activity measured in the HO-derived supernatant is explained by the instability and/or activation of the FVII protein in the serum-free cell medium with consequent functional degradation, complex formation, or other forms of inhibition[19,38,39] remains to be thoroughly investigated.

In this study, PH were included as a positive control rather than as a benchmark comparator for therapeutic performance. Unlike HO, which recapitulate the multicellular architecture and complexity of the liver, PH represent a highly purified monolayer of terminally differentiated primary hepatocytes, cultured at high density in low-volume conditions for only a few days. These fundamental differences in cell composition, density, and media volume limited the direct comparisons in terms of absolute secretion or functional output. To address this and accurately characterize functional output, we calculated the specific activity (mIUng) by normalizing measured FVII:C to FVII:Ag levels and confirmed that the protein secreted by corrected HO was functionally active. To expand on this further, the thrombin generation assays provided additional functional insight, demonstrating a more substantial correction of the overall coagulation profile. This assay provides a comprehensive view of the coagulation kinetic by measuring thrombin generation over time in FVII-deficient plasma supplemented with HO-derived supernatant. The marked reduction in lag time suggested that the restored FVII secretion translated into biologically functional activity. Notably, these results also indicate that the rescued FVII protein underwent the post-translational modifications that are required for proper secretion and biological function.[40-43] However, the clinical relevance of this rescue remains to be further investigated. The HO production can be exponentially expanded offering the potential to generate therapeutically relevant quantities for transplantation.[9] In this perspective, although the capacity of HO to engraft and sustain long-term secretion of human liver proteins *in vivo* has already been demonstrated by Harrison *et al*.,[9] the next essential objective of this study will be to assess therapeutic efficacy in a disease-relevant *in vivo* model.

In conclusion, we demonstrate the first *in vitro* correction of severe FVII deficiency, using patient-derived, CRISPR-corrected liver organoids. Our study presents a proof of principle in the development of a novel cell therapy for FVII deficiency, with potential applicability across the spectrum of inherited coagulation factor deficiencies.

Disclosures

GJS is the co-founder and CSO of Occam BioSciences Ltd. GJS and SPH are holders of the liver organoid technology used in this study (patent WO2022101675A1). All other authors have no conflicts of interest to disclose.

Contributions

GR performed experiments, analyzed the data and wrote the manuscript. BSt, MEC, MSA, MCM, AB, BSm and SPH participated in performing the experiments. HG recruited the patient. KHL, CEH and NI participated in data analysis and revised the manuscript. RA contributed to the single-cell cloning experiments and revised the manuscript. BT performed the LC-MS experiments. GJS, BSt, PMS and MEC conceived and designed the study, participated in the data analysis and revised the manuscript. All authors approved the final version.

Acknowledgments

The authors would like to thank Ellen Skarpen at the Core Facility for Advanced Light Microscopy, Institute for Cancer Research, Oslo University Hospital, for assistance with the confocal microscopy.

Funding

This study was funded by the Norwegian Research Council (325869).

Data-sharing statement

The data analyzed in this study are available from the corresponding author upon reasonable request.

References

1. Chollet ME, Andersen E, Skarpen E, et al. Factor VII deficiency: unveiling the cellular and molecular mechanisms underlying three model alterations of the enzyme catalytic domain. Biochim Biophys Acta Mol Basis Dis. 2018;1864(3):660-667.
2. Andersen E, Chollet ME, Sletten M, et al. Molecular characterization of two homozygous factor VII variants associated with intracranial bleeding. Thromb Haemost. 2021;121(12):1588-1598.
3. Mariani G, Herrmann FH, Dolce A, et al. Clinical phenotypes and factor VII genotype in congenital factor VII deficiency. Thromb Haemost. 2005;93(3):481-487.
4. Napolitano M, Siragusa S, Mariani G. Factor VII deficiency: clinical phenotype, genotype and therapy. J Clin Med. 2017;6(4):38.
5. Robinson KS. An overview of inherited factor VII deficiency. Transfus Apher Sci. 2019;58(5):569-571.
6. Bernardi F, Dolce A, Pinotti M, et al. Major differences in bleeding symptoms between factor VII deficiency and hemophilia B. J Thromb Haemost. 2009;7(5):774-779.
7. Si-Tayeb K, Noto FK, Nagaoka M, et al. Highly efficient generation of human hepatocyte-like cells from induced pluripotent stem cells. Hepatology. 2010;51(1):297-305.
8. Sullivan GJ, Hay DC, Park IH, et al. Generation of functional human hepatic endoderm from human induced pluripotent stem cells. Hepatology. 2010;51(1):329-335.
9. Harrison SP, Siller R, Tanaka Y, et al. Scalable production of tissue-like vascularized liver organoids from human PSCs. Exp Mol Med. 2023;55(9):2005-2024.
10. Mathapati S, Siller R, Impellizzeri AAR, et al. Small-molecule-directed hepatocyte-like cell differentiation of human pluripotent stem cells. Curr Protoc Stem Cell Biol. 2016;2016(1):1G.6.1-1G.6.18.
11. Lian X, Zhang J, Azarin SM, et al. Directed cardiomyocyte differentiation from human pluripotent stem cells by modulating Wnt/β-catenin signaling under fully defined conditions. Nat Protoc. 2013;8(1):162-175.
12. Chambers SM, Fasano CA, Papapetrou EP, Tomishima M, Sadelain M, Studer L. Highly efficient neural conversion of human ES and iPS cells by dual inhibition of SMAD signaling. Nat Biotechnol. 2009;27(3):275-280.
13. Maroof AM, Keros S, Tyson JA, et al. Directed differentiation and functional maturation of cortical interneurons from human embryonic stem cells. Cell Stem Cell. 2013;12(5):559-572.
14. Zhang M, Ngo J, Pirozzi F, Sun YP, Wynshaw-Boris A. Highly efficient methods to obtain homogeneous dorsal neural progenitor cells from human and mouse embryonic stem cells and induced pluripotent stem cells. Stem Cell Res Ther. 2018;9(1):1-13.
15. Peters DT, Henderson CA, Warren CR, et al. Asialoglycoprotein receptor 1 is a specific cell-surface marker for isolating hepatocytes derived from human pluripotent stem cells. Development. 2016;143(9):1475-1481.
16. Son JS, Park CY, Lee G, et al. Therapeutic correction of hemophilia A using 2D endothelial cells and multicellular 3D organoids derived from CRISPR/Cas9-engineered patient iPSCs. Biomaterials. 2022;283:121429.
17. Lyu C, Shen J, Wang R, et al. Targeted genome engineering in human induced pluripotent stem cells from patients with hemophilia B using the CRISPR-Cas9 system. Stem Cell Res Ther. 2018;9(1):92.
18. Ramaswamy S, Tonnu N, Menon T, et al. Autologous and heterologous cell therapy for hemophilia B toward functional restoration of factor IX. Cell Rep. 2018;23(5):1565-1580.
19. Luce E, Steichen C, Allouche M, et al. In vitro recovery of FIX clotting activity as a marker of highly functional hepatocytes in a hemophilia B iPSC model. Hepatology. 2022;75(4):866-880.
20. Park CY, Kim DH, Son JS, et al. Functional correction of large factor VIII gene chromosomal inversions in hemophilia A patient-derived iPSCs using CRISPR-Cas9. Cell Stem Cell. 2015;17(2):213-220.
21. Giansily-Blaizot M, Rallapalli PM, Perkins SJ, et al. The EAHAD blood coagulation factor VII variant database. Hum Mutat. 2020;41(7):1209-1219.
22. Landau D, Rosenberg N, Zivelin A, Staretz-Chacham O, Kapelushnik J. Familial factor VII deficiency with foetal and neonatal fatal cerebral haemorrhage associated with homozygosis to Gly180Arg mutation. Haemophilia. 2009;15(3):774-778.
23. Giansily-Blaizot M, Aguilar-Martinez P, Biron-Andreani C, et al. Analysis of the genotypes and phenotypes of 37 unrelated patients with inherited factor VII deficiency. Eur J Hum Genet. 2001;9(2):105-112.

24. Kuperman AA, Barg AA, Fruchtman Y, et al. Primary prophylaxis for children with severe congenital factor VII deficiency - clinical and laboratory assessment. Blood Cells Mol Dis. 2017;67:86-90.
25. Pacesa M, Pelea O, Jinek M. Past, present, and future of CRISPR genome editing technologies. Cell. 2024;187(5):1076-1100.
26. DeWitt MA, Corn JE, Carroll D. Genome editing via delivery of Cas9 ribonucleoprotein. Methods. 2017;121-122:9-15.
27. Vakulskas CA, Dever DP, Rettig GR, et al. A high-fidelity Cas9 mutant delivered as a ribonucleoprotein complex enables efficient gene editing in human hematopoietic stem and progenitor cells. Nat Med. 2018;24(8):1216-1224.
28. Kim S, Kim D, Cho SW, Kim J, Kim J-S. Highly efficient RNA-guided genome editing in human cells via delivery of purified Cas9 ribonucleoproteins. Genome Res. 2014;24(6):1012-1019.
29. Chen PJ, Liu DR. Prime editing for precise and highly versatile genome manipulation. Nat Rev Genet. 2023;24(3):161-177.
30. Li C, Georgakopoulou A, Newby GA, et al. In vivo HSC prime editing rescues sickle cell disease in a mouse model. Blood. 2023;141(17):2085-2099.
31. Zeng J, Wu Y, Ren C, et al. Therapeutic base editing of human hematopoietic stem cells. Nat Med. 2020;26(4):535-541.
32. Parums DV. Editorial: First regulatory approvals for CRISPRCas9 therapeutic gene editing for sickle cell disease and transfusion-dependent β-thalassemia. Med Sci Monit. 2024;30:e944204.
33. Tristan CA, Hong H, Jethmalani Y, et al. Efficient and safe single-cell cloning of human pluripotent stem cells using the CEPT cocktail. Nat Protoc. 2023;18(1):58-80.
34. Chen YH, Pruett-Miller SM. Improving single-cell cloning workflow for gene editing in human pluripotent stem cells. Stem Cell Res. 2018;31:186-192.
35. Singh AM. An efficient protocol for single-cell cloning human pluripotent stem cells. Front Cell Dev Biol. 2019;7:11.
36. Zhang Y, Jiang Q, Liang X, et al. Coagulation factor VII fine-tunes hepatic steatosis by blocking AKT-CD36-mediated fatty acid uptake. Diabetes. 2024;73(5):682-700.
37. Zabulica M, Srinivasan RC, Vosough M, et al. Guide to the assessment of mature liver gene expression in stem cell-derived hepatocytes. Stem Cells Dev. 2019;28(14):907-919.
38. Lengler J, Coulibaly S, Gruber B, et al. Development of an in vitro biopotency assay for an AAV8 hemophilia B gene therapy vector suitable for clinical product release. Mol Ther Methods Clin Dev. 2020;17:581-588.
39. Nederlof A, Kitchen S, Meijer P, et al. Performance of factor IX extended half-life product measurements in external quality control assessment programs. J Thromb Haemost. 2020;18(8):1874-1883.
40. Bolt G, Steenstrup TD, Kristensen C. All post-translational modifications except propeptide cleavage are required for optimal secretion of coagulation factor VII. Thromb Haemost. 2007;98(5):988-997.
41. Bolt G, Kristensen C, Steenstrup TD. More than one intracellular processing bottleneck delays the secretion of coagulation factor VII. Thromb Haemost. 2008;100(2):204-210.
42. Clarke BJ, Sridhara S. Incomplete gamma carboxylation of human coagulation factor VII: differential effects on tissue factor binding and enzymatic activity. Br J Haematol 1996;93(2):445-450.
43. Wang H, Wang L, Li S, Dong N, Wu Q. N-Glycan-calnexin interactions in human factor VII secretion and deficiency. Int J Biochem Cell Biol. 2019;113:67-74.
44. Mathijssen NCJ, Masereeuw R, Holme PA, et al. Increased volume of distribution for recombinant activated factor VII and longer plasma-derived factor VII half-life may explain their long lasting prophylactic effect. Thromb Res. 2013;132(2):256-262.